A Comparative Study of Numerical Advection Schemes Featuring a One-Step Modified WKL Algorithm

CHING-YUANG HUANG AND SETHU RAMAN

Department of Marine, Earth, and Atmospheric Sciences, North Carolina State University, Raleigh, North Carolina

(Manuscript received 11 June 1990, in final form 1 April 1991)

ABSTRACT

A fourth-order Crowley-type advection scheme based on the multistep Warming–Kutler–Lomax (WKL) scheme is proposed in this study. This scheme utilizes a free parameter to minimize dispersion and dissipation and can be used to represent the advection of positive-definite scalars (such as moisture).

Linear Fourier component analyses indicate that the fourth-order Crowley-type scheme can reproduce the features of other modified Crowley-type schemes of third order, such as the scheme of Schlesinger and the quadratic upstream interpolation. Using the free parameter, the scheme may illustrate the limitation of the Crowley-type schemes for which diffusion is required for numerical stability of advective quantity. For these schemes, formulations that preserve amplitude are inevitably associated with smaller time steps. Adding the first cross-space term into these schemes could eliminate marginal instability or overshooting in linear advection.

Linear and nonlinear advection tests show that the performance of the proposed scheme is comparable to the fourth-order leapfrog scheme (which requires more computer memory) and the cubic upstream spline (which requires more computer time). This two-time-level advection scheme can thus be used in a numerical model to save computer resources.

1. Introduction

The second-order Crowley advection scheme (Crowley 1968) has been widely used in two-time-level numerical models for many years (Smolarkiewicz 1982). Remarkable features of this scheme are well known and have been discussed in previous papers (Fromm 1969; Petschek and Libersky 1975; Smolarkiewicz 1982; Schlesinger 1985). Its main shortcoming is the strong dispersion that leads to instability in long-term advection. Petschek and Libersky (1975) showed that this scheme was theoretically unstable for two-dimensional (2D) advection because the maximum magnitude of its associated eigenvalues (the amplification factor) is greater than unity. The time-splitting Crowley scheme that represents each directional advection separately in time becomes stable for uniform flow (Leith 1965). However, the scheme remains weakly unstable in the case of deformational flow (Petschek and Libersky 1975). The modified second-order Crowley schemes mentioned above still exhibit strong dispersion (Smolarkiewicz 1982; Schlesinger 1985).

To reduce the strong dispersion associated with the second-order Crowley schemes mentioned above, Schlesinger (1985) added an upstream-biased third-order phase correction term that is based on the Taylor's expansions of the first spatial partial derivative. This modified scheme was shown to preserve significantly better phase but slightly worse amplitude compared with those for the second-order Crowley schemes. The quadratic upstream interpolation of third-order accuracy (Leonard 1979) preserves amplitude better than Schlesinger's scheme, since it does not retain the second-order diffusion term of the latter. The upstream-biased quadratic interpolation implies implicit diffusion and may be considered as one of the Crowley-type schemes in which diffusion is required for advective stability. The diffusion is used to stabilize advection in finite-difference forms that are forward in time and centered in space (FTCS). Both Schlesinger's scheme and the quadratic upstream interpolation of third order preserve phase much better than second-order Crowley schemes. But, they still produce less accurate amplitudes than the fourth-order leapfrog scheme, which is a three-time-level formulation (Haltiner and Williams 1980), and the cubic upstream spline, which requires matrix computation (Purnell 1976; Mahrer and Pielke 1978). This will be shown later in this paper.

One objective of this paper is to investigate the performance of different advection schemes in both linear and nonlinear advection. To alleviate the major shortcoming of the second-order and third-order Crowley-type schemes discussed above, we propose a fourth-order Crowley-type scheme. We will show that the performance of this scheme is comparable to the fourth-order leapfrog scheme and the cubic upstream

Corresponding author address: Dr. Sethu Raman, Dept. of Marine, Earth, and Atmosphere Sciences, North Carolina State University, Raleigh, NC 27695-8208.

spline in both linear and nonlinear advection. Since the finite-difference formulation of this Crowley-type scheme is simple and involves two time levels, it can save computer costs. In this study, the effects of cross-space terms on the performance of the advection schemes are also investigated. The first cross-space term of second order has been shown to enhance the numerical performance of the Crowley-type schemes (Smolarkiewicz 1982; Schlesinger 1985). The cross-space term of second order is a portion of the time truncation error in multidimensional Crowley-type schemes and is proportional to second-order mixed spatial or "cross" partial derivatives of the advected quantity. Numerical results of linear advection in uniform and rotational flows are given in section 3. Linear Fourier component analyses for the proposed scheme are discussed in section 4. In addition to the theoretical analyses, the reliability of the scheme in the simulation of nonlinear mountain waves is examined using a primitive equation numerical model.

2. Numerical schemes and other components

Linear advection of a scalar ϕ for 2D flow is governed by

$$\frac{\partial \phi}{\partial t} + U\frac{\partial \phi}{\partial x} + V\frac{\partial \phi}{\partial y} = 0, \tag{1}$$

where U and V are the wind components in the x and y directions, respectively. In this study, the flow is assumed to be nondivergent and steady. The advection equation can be solved numerically at discrete grid points, and computational stability is related to the Courant number defined as

$$\nu = (\alpha^2 + \beta^2)^{1/2}, \tag{2}$$

with the directional Courant numbers in the respective x and y directions given by

$$\alpha = \frac{U_{i,j}\Delta t}{\Delta x}, \quad \beta = \frac{V_{i,j}\Delta t}{\Delta y}, \tag{3}$$

where indices i and j denote a discrete grid in the respective x and y directions, Δt is the time step, and Δx and Δy are constant grid intervals.

a. Numerical schemes

We consider only the finite-difference advection schemes that are commonly used in meteorological numerical models. The advection schemes tested in this study are the following.

- L0 the second-order and fourth-order leapfrog schemes
- L1 the first-order upstream scheme
- L2 the quadratic upstream interpolation (Leonard 1979a,b)
- L3 the cubic upstream spline
- L4 the second-order upstream (upwind) scheme (Warming and Beam 1975)
- L5 the Crowley scheme or Lax–Wendroff scheme (Crowley 1968; Lax and Wendroff 1960)
- L5M the modified Crowley scheme (Anderson et al. 1984)
- L6 the Crowley scheme with the third-order phase correction (Schlesinger 1985)
- L7 the Warming–Kutler–Lomax (WKL) scheme (Warming et al. 1973)
- L8 the modified WKL scheme (proposed)
- L8M the modified WKL with selective control (proposed)

Finite-difference forms for the schemes L0, L1, L2, L4, L5, and L7 can be found in Anderson et al. (1984). The scheme L3 in which the time-splitting formulation is used to simplify the 2D computation was discussed by Pielke (1984). For L5M, the original second-order Crowley scheme (or the Lax–Wendroff scheme) can be modified simply by adding the negative of its third-order differential term in its error-indication equation (see Anderson et al. 1984) into the original scheme. Thus, this scheme is third-order accurate. Scheme L6 is equivalent to Schlesinger's scheme 4 with the type I correction (an upstream-biased third-order phase correction). This scheme remedies the dispersion caused by the first-order term in L5. Scheme L5M is similar to L6, but the third-order correction term is centered and has different leading coefficients. Scheme L2 is identical to the scheme L6 if the second-order term of the latter is dropped. Note that L2 is not fully upstream differenced since it involves one downstream grid point.

Scheme L7 (the WKL scheme) is a three-step scheme. Its 1D formulation is given by

$$\textit{step 1: } \phi_i^* = \phi_i^n - \frac{2}{3}\alpha(\phi_{i+1}^n - \phi_i^n)$$

$$\textit{step 2: } \phi_i^{**} = \frac{1}{2}\left[\phi_i^n + \phi_i^* - \frac{2}{3}\alpha(\phi_i^* - \phi_{i-1}^*)\right]$$

$$\textit{step 3: } \phi_i^{n+1} = \phi_i^n - \frac{1}{24}\alpha(-2\phi_{i+2}^n + 7\phi_{i+1}^n - 7\phi_{i-1}^n + 2\phi_{i-2}^n) - \frac{3}{8}\alpha(\phi_{i+1}^{**} - \phi_{i-1}^{**}) - \frac{\omega}{24}(\phi_{i+2}^n - 4\phi_{i+1}^n + 6\phi_i^n - 4\phi_{i-1}^n + \phi_{i-2}^n), \tag{4}$$

where ω is a free parameter added for stability. Index i refers to the grid point in the corresponding direction. This scheme has the error-indication equation (see Anderson et al. 1984) given by

$$\phi_t + U\phi_x = -\frac{U(\Delta x)^3}{24}\left(\frac{\omega}{\alpha} - 4\alpha + \alpha^3\right)\phi_{xxxx} + \frac{U(\Delta x)^4}{120}(-5\omega + 4 + 15\alpha^2 - 4\alpha^4)\phi_{xxxxx} + O[(\Delta x)^5]. \quad (5)$$

This scheme is stable if

$$|\alpha| \leq 1 \quad \text{and} \quad 4\alpha^2 - \alpha^4 \leq \omega \leq 3, \quad (6)$$

as shown by Anderson and Fattahi (1974). The scheme has minimum dissipation with

$$\omega = \omega_1 = 4\alpha^2 - \alpha^4, \quad (7)$$

which causes the coefficient of the fourth-order derivative ϕ_{xxxx} to vanish, and minimum dispersion with

$$\omega = \omega_2 = \frac{(4\alpha^2 + 1)(4 - \alpha^2)}{5}, \quad (8)$$

which eliminates the fifth-order derivative. The scheme thus is fourth-order accurate with least dissipation and third-order accurate with least dispersion.

The original WKL scheme can be reduced to a one-step scheme if the updated values of ϕ at step 1 and step 2 in (4) are taken into step 3. The one-step WKL scheme then has the final form

$$\phi_i^{n+1} = \phi_i^n - \frac{\alpha}{12}(-\phi_{i+2}^n + 8\phi_{i+1}^n - 8\phi_{i-1}^n + \phi_{i-2}^n) + \frac{\alpha^2}{8}(\phi_{i+2}^n - 2\phi_i^n + \phi_{i-2}^n) + \frac{\alpha^3}{12}(-\phi_{i+2}^n + 2\phi_{i+1}^n - 2\phi_{i-1}^n + \phi_{i-2}^n) - \frac{\omega}{24}(\phi_{i+2}^n - 4\phi_{i+1}^n + 6\phi_i^n - 4\phi_{i-1}^n + \phi_{i-2}^n). \quad (9)$$

The term involving α^3 may be neglected without losing accuracy since $\alpha^3/12$ is much smaller than other leading coefficients for values of α much less than unity. It will be shown in section 4 that for 2D flow α must be less than approximately 0.35 for the stability of the scheme; however, one should probably retain the term in α^3 for 1D flow, although it would involve more computation. Hence, a modified WKL scheme (L8) is proposed with a free parameter ω ranging between

$$\omega_1 = 4\alpha^2 \quad (10)$$

and

$$\omega_2 = 0.8(4\alpha^2 + 1). \quad (11)$$

Selective dispersion and dissipation controlled by this free parameter become possible if

$$\omega = \omega_1, \quad \text{for} \quad \phi_i^n > 0$$
$$\omega = \omega_2, \quad \text{for} \quad \phi_i^n \leq 0. \quad (12)$$

Features discussed above form the basis of the proposed scheme (L8M) for positive definite scalars. Since negative values could be generated by numerical dispersion, these values must be reset to zero, in addition to the use of the scheme L8M. According to (12), heavy damping with $\omega = \omega_2$ is also applied to places where zero values exist.

Anderson et al. (1984) have given detailed 1D stability analyses of L0, L1, L4, L5, and L7. Haltiner and Williams (1980) also discussed stabilities of L0, L1, and L5. Interested readers may refer to Leonard (1979) for L2, Pielke (1984) for L3, and Schlesinger (1985) for L6. The 2D stability of the modified WKL scheme (L8) with the first cross-space term (given below) will be investigated in section 4 using Fourier component analyses.

b. *Other numerical components*

Cross-space terms were usually neglected in weather prediction models, probably because they were considered to have little effect on the performance of an advection scheme. Smolarkiewicz (1982) showed that the first cross-space term of second order in the Taylor's expansion of the original Crowley scheme can increase its stability range and therefore significantly improve its long-term performance. However, Schlesinger (1985) found that the effects of the second-order cross-space term in various flow advection tests are not as obvious. This contradiction indicates a need to further examine the effects of cross-space terms on the performance of an advection scheme. Since a lower-order correction is more important than a higher-order correction, only the first cross-space term of second order,

$$C_{i,j}^n = \frac{1}{4}\alpha\beta(\phi_{i+1,j+1}^n - \phi_{i-1,j+1}^n - \phi_{i+1,j-1}^n + \phi_{i-1,j-1}^n), \quad (13)$$

will be examined. This first cross-space term has an error of $O[(\Delta x)^2, (\Delta y)^2]$.

To investigate the effect of a numerical smoother on linear advection, we select the fourth-order linear filter proposed by Shapiro (1971). Waves of two grid intervals will be completely eliminated at each time step by applying this linear filter twice with a filter parameter $S = 0.125$ the first time and $S = -0.125$ the second time. The filter thus controls the aliasing errors in nonlinear advection and is the most widely used one in meteorological numerical models.

A time smoothing is required for the leapfrog scheme because of its three-time-level formulation that inevitably generates splitting computational modes (Mesinger and Arakawa 1976). Robert's (1966) time

smoothing with a filter coefficient μ is thus used to reduce the splitting tendency of the solutions for the leapfrog scheme. Haltiner and Williams (1980) have discussed the detailed features of both the linear filter and the time smoothing.

The lateral boundary condition used in this paper is a radiation condition (Miller and Thorpe 1981),

$$\phi_b^{n+1} = \phi_b^n - r(\phi_b^n - \phi_{b1}^n),$$

$$r = (\phi_{b1}^{n+1} - \phi_{b1}^n)(\phi_{b2}^n - \phi_{b1}^n)^{-1} \quad \text{for} \quad 0 \leq r \leq 1,$$

where subscripts b, $b1$, and $b2$ indicate a boundary grid point, and the first and second grid points adjacent to the boundary, respectively. In addition, the upstream scheme is used at the grid points adjacent to boundaries for the modified WKL scheme and the cubic upstream spline. It has been found that this approach enhances the performance of the advection schemes near boundaries.

3. Linear advection tests

In this study, uniform flow (UL) and rotational flow (RL) were chosen to test advection schemes. Following Long and Pepper (1976), the initial distribution of a scalar ϕ in a cone-shaped hill as

$$\phi_{i,j} = \begin{cases} 50\left[1 + \cos\left(\dfrac{\pi R_{i,j}}{4H}\right)\right], & R_{i,j} \leq 4H \\ 0, & R_{i,j} > 4H, \end{cases} \quad (14)$$

was chosen with

$$R_{i,j} = [(x_i - x_p)^2 + (y_j - y_p)^2]^{1/2} \quad (15)$$

for a given peak at (x_p, y_p), and H is set to the grid interval. Three-dimensional (3D) surface curves of the two imposed hills in the uniform flow (UL) test are plotted in Fig. 1. The wind velocity components $U_{i,j}$ and $V_{i,j}$ are 5 m s^{-1} in the UL test, and

$$U_{i,j} = -(y_j - y_c)\Omega, \quad V_{i,j} = (x_i - x_c)\Omega \quad (16)$$

in the RL test. The grid indices for the center of rotation (x_c, y_c) are (20, 20) with a constant angular velocity, $\Omega = 2\pi/10\,800$ s^{-1} (i.e., 3 h for one revolution). Constant grid intervals $\Delta x = \Delta y = \Delta$ are 5 km for both tests, with an integration time step Δt of 60 s in the UL test and 15 s in the RL test. In the RL test, the maximum wind speed is about 82 m s^{-1}, which may occur in strong tornadoes or extreme hurricanes at the surface and a strong upper-tropospheric jet streak. The maximum directional Courant numbers α and β are equal to 0.06 in the UL test and 0.175 in the RL test. Initially, the centers of the two hills in the UL test are on grid points (14, 14) and (20, 20) and the center of the hill in the RL test is on grid point (15, 15). The uniform flow blows diagonally toward the grid point (40, 40), while the rotational flow turns around the central grid point (20, 20).

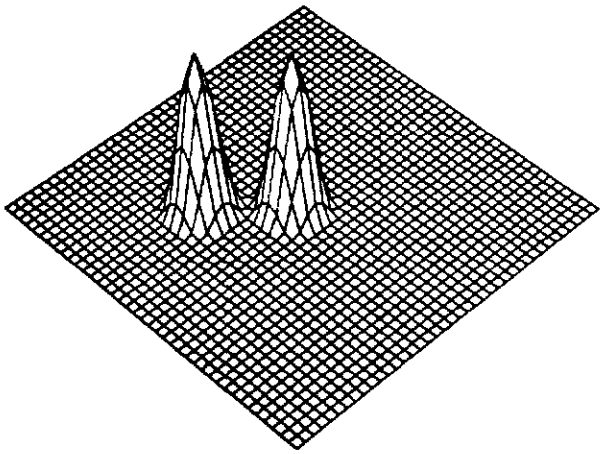

FIG. 1. The initial condition for the linear advection with uniform flow. Gridpoint numbers (i, j) range from (1, 1) to (40, 40). The two hill peaks have the height of 100 units as reference. one peak located at (14, 14) and the other at (20, 20). The viewing angles are −45° for horizontal projection and 45° for vertical projection (downward), so the grid point (1, 1) is on the left edge of the figure and the grid point (40, 40) on the right edge of figure. Uniform grid intervals with $\Delta x = \Delta y = 5$ km and $\Delta t = 60$ s are used in this test.

The numerical results for the fourth-order leapfrog scheme associated with the radiation boundary condition are given in Fig. 2. To suppress the computational mode generated by the three-time-level formulation, a time filter coefficient μ of 0.05 was used. The second-order leapfrog scheme yields significant dispersion of long waves, which leads to a maximum amplitude only about 80% of the initial value at 6 h (see Fig. 3a for similar results). The fourth-order leapfrog scheme preserves the maximum amplitude to approximately 90% at 6 h and, in general, gives much better phase accuracy than the second-order scheme. Some shorter dispersive waves still appear near the hill and far upstream for the fourth-order scheme because of its computational mode (Haltiner and Williams 1980). The upstream dispersive waves can be suppressed using a larger filter coefficient μ.

The first-order upstream scheme is usually compared with the second-order leapfrog scheme since both have the same maximum Courant number for stability (Pielke 1984). Strong dissipation associated with the first-order upstream scheme (L1) results in an amplitude that is almost fully suppressed at 6 h (not shown) in the UL test. The second-order upstream scheme (L4) has moderate dissipation and dispersion (mainly for leading phase error) and preserves only about 50% of the initial maximum amplitude at 6 h (not shown).

The results at 3 h for the original Crowley scheme (L5) and Schlesinger's scheme (L6) are given in Fig. 3. Scheme L5 performs in a manner similar to the second-order leapfrog scheme, with severely lagging phase dispersion behind the hills. In contrast, little dispersion is produced by L6 with the third-order phase correction.

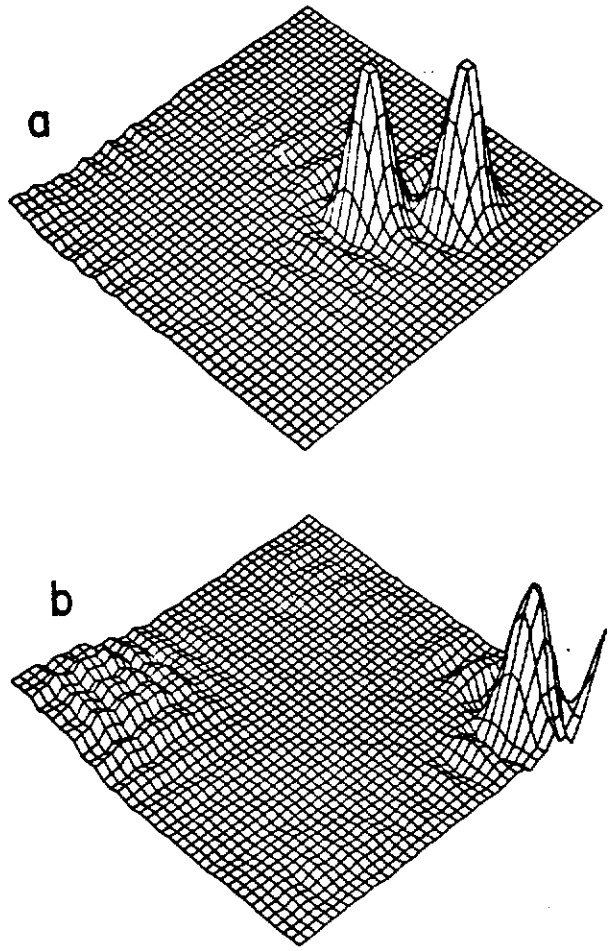

FIG. 2. The results in the uniform flow test for the fourth-order leapfrog scheme (L0) at (a) 3 h and (b) 6 h.

In the UL test, L5 is stable, despite the fact that its maximum eigenvalue exceeds unity (Fromm 1969; Petschek and Libersky 1975). Although L6 preserves phase much better than L5, this scheme preserves only 60% of the amplitude at 6 h compared to 80% for L5. With the third-order correction based on the error-indication equation of the original Crowley scheme, L5M preserves amplitude much better than L6 (not shown). It has been found that the results for L5M were near identical to those for L0, except for the upstream dispersive waves that appear in L0.

The results for the quadratic upstream interpolation (L2) and the cubic upstream spline (L3) are shown in Fig. 4. As can be seen, the two schemes preserve both phase and amplitude well. Scheme L2 preserves 85% amplitude at 6 h, comparable to the results of the fourth-order leapfrog scheme (L0). Scheme L3 is a global one (using all grid information) and thus gives a maximum amplitude of more than 95%. The maximum amplitude for L3, however, tends to slightly overshoot as the hills approach the corner of the domain.

According to the results of the UL test, L0 is not comparable to L3. In practice, L3 preserves phase and amplitude better than L0, although L0 is a neutral, nondamping scheme (Haltiner and Williams 1980). Figure 5 shows the results for L0 and L3 after one full rotation (3 h) in the RL test. In the RL test, L3 is better than L0 in the preservation of phase, with only slight dispersion near the hill. In amplitude, L3 gives a maximum value of 95% while it is about 85% for L0. No overshooting is found for the scheme L3 in this test. The other upstream-biased third-order scheme L2 preserves slightly lower amplitude but better phase (not shown) as compared to L0, similar to their performance in the UL test. Scheme L6 preserves a maximum amplitude of only 55% compared to 70% for L2.

The results in the UL and RL tests for the multiple-step WKL scheme L7 (with the free parameter $\omega = \omega_1$ for least dissipation) appear to be near identical to those

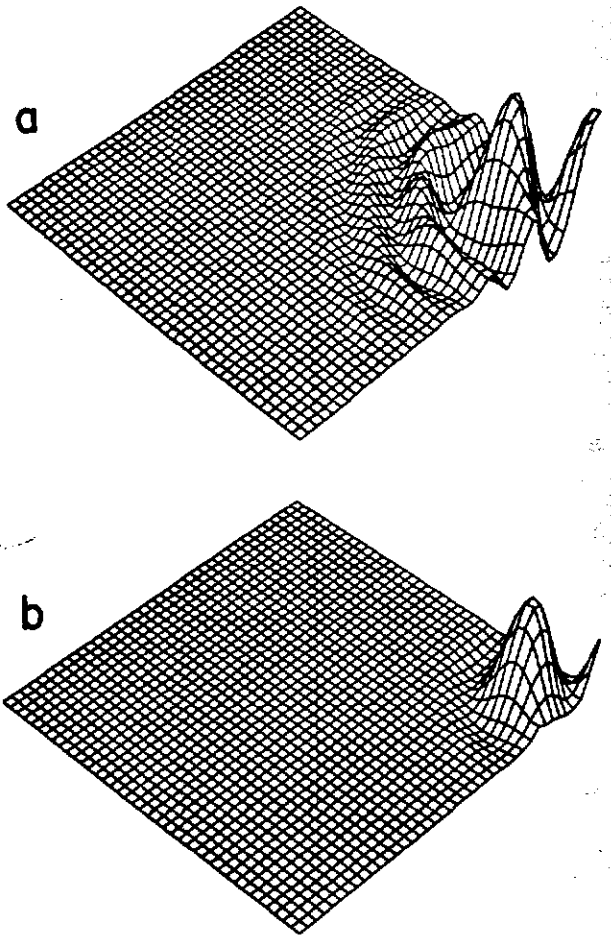

FIG. 3. As in Fig. 2 but at 6 h for schemes (a) L5 and (b) L6 (for descriptions of the schemes see text).

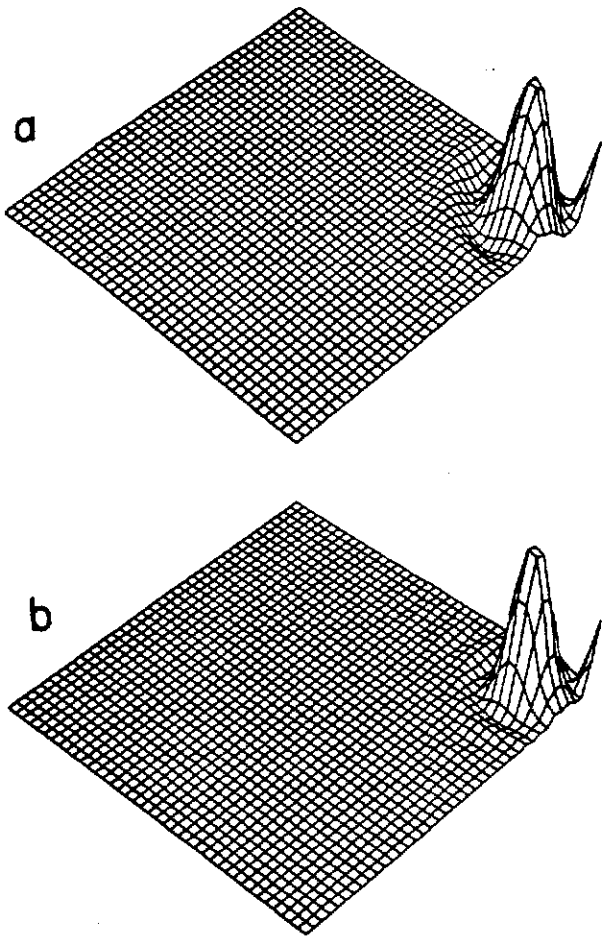

FIG. 4. As in Fig. 2 but at 6 h for schemes (a) L2 and (b) L3.

for the one-step schemes L5M and L0. In fact, it was found that all higher-order schemes L0, L5M, L7, and even L8 preserve nearly identical amplitude for scalars without positive definiteness, despite slight differences in their dispersion. For positive definite scalars, the performance of L8M (with the cross-space term) is better than other schemes because of the selective control of dispersion as evident in Fig. 6. Note that for positive definite scalars, negative values are reset to zero after advection at a new time step. This resetting tends to act as a source of the advective quantity. No compensation through the reduction of other positive values is made to better conserve the initial quantity. According to the selective control [Eq. (12)] in L8M, heavy damping is applied to grid points where zero values exist. The heavy damping will also reduce the magnitude of positive values adjacent to the regions of zero values and, thus, possibly acts to compensate. For this case, L8M (with and without the cross-space term) performs in a satisfactory manner as compared to a more complex scheme L3 (Fig. 6). As can be seen in this figure, the original shapes are truthfully preserved by the two schemes. For this short-term test, the cross-space term does not influence the performance of L8M; however, it will be shown later that without this term its performance will degrade as more rotations progress.

Before examining the long-term performance of the schemes, the effects of the first cross-space term should be briefly shown. Without this term, schemes L2 (with Δt = 120 s), L5M (with Δt = 240 s), and L6 (with Δt = 360 s) exhibit overshooting or instability at 3 h in the UL test. Once the cross-space term is included, the three schemes become stable. An example for L6 is shown in Fig. 7. The cross-space term gives a wider stability range and thus improves the results for flow regimes with marginal stability. However, this modification does not improve the results for a smaller Courant number (e.g., with Δt less than 60 s). The results are not sensitive to the cross-space term as long as the time step is not close to the critical value that could cause overshoot or instability. The role of the cross-space term will be further analyzed using Fourier components in section 4.

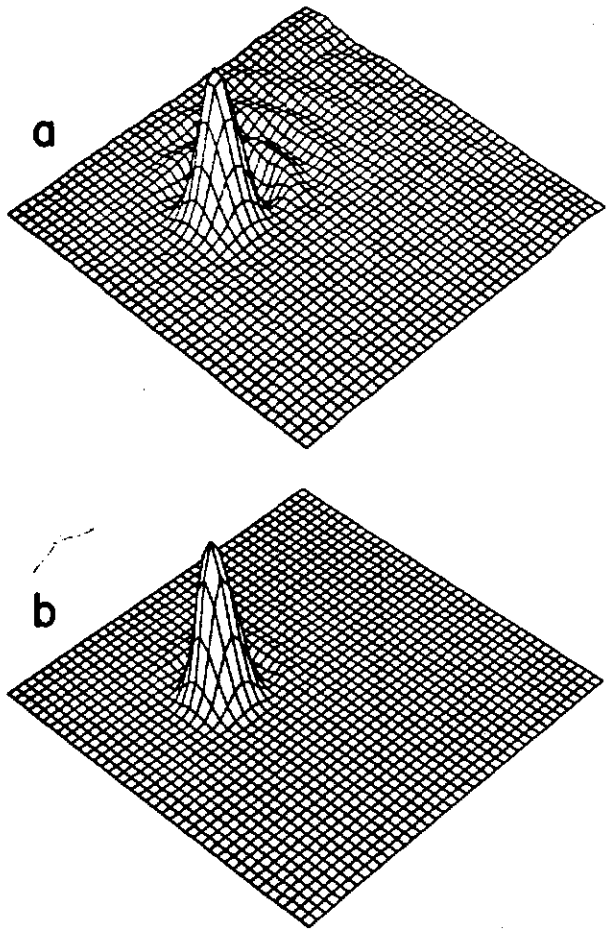

FIG. 5. The results at 3 h in the rotation flow test for schemes (a) L0 and (b) L3.

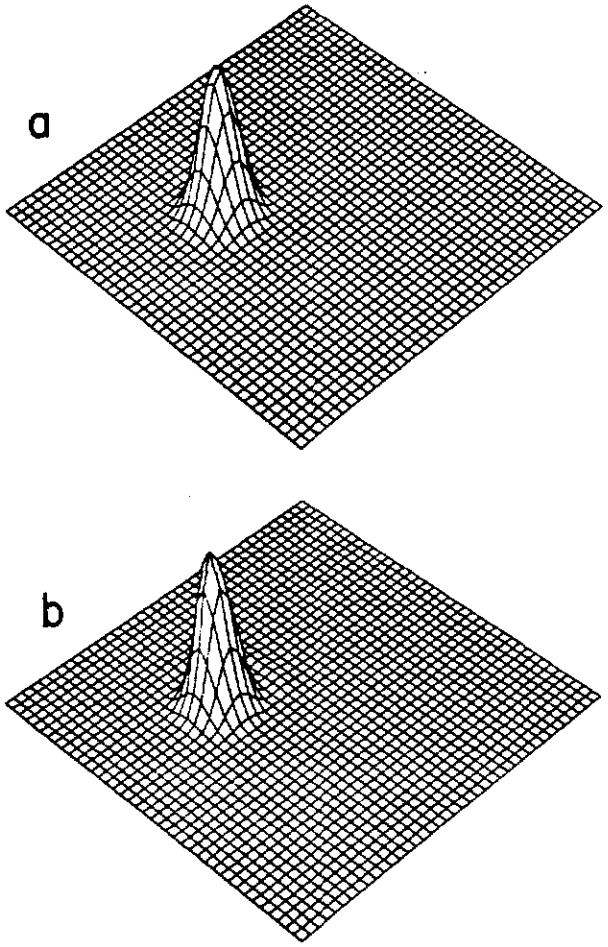

FIG. 6. The results at 3 h in the rotational flow test for positive definite scalars using schemes (a) L8M and (b) L3.

The results after four full rotations (12 h) in the RL test for schemes L0, L3, and L8M for positive-definite scalars are shown in Fig. 8. For positive-definite scalars, the results for L0 with $\mu = 0.2$ show some moderate dispersion of positive values near the hill. Scheme L3 gives only slight dispersion near the hill for scalars either with or without definite positiveness. For L8M (without the cross-space term), the initial shape has broadened considerably at 12 h. This feature becomes less noticeable with the inclusion of the cross-space term. Despite the gradually widened shape, there is no dispersion around the hill during the integration. With the cross-space term, the scheme L8M is more comparable to L3 than other schemes in preserving both amplitude and phase of the hill.

Table 1 gives a review of the maximum amplitudes and the features of dispersion for the schemes used in the long-term RL test. In this table, the characters C and P, adjacent to the scheme's name, indicate the inclusion of the cross-space term and the advection of positive-definite scalars, respectively. Dispersion for the schemes are graded from degree A (best) to degree F (worst). After four rotations, the fourth-order leapfrog scheme (L0) with weak smoothing suffers severe dispersion everywhere (degree F). This may be remedied by applying the space filter or using a larger time coefficient according to Table 1. Use of the linear filter is thus necessary for L0 to obtain slight dispersion near the hill (degree B). The quadratic upstream interpolation (L2) is unstable in this long-term test, although it is stable in the short term. The scheme becomes stable once the cross-space term is included, indicating the importance of this term in stabilizing numerical advection in the rotational flow. The cubic upstream spline (L3) is also stable and preserves amplitude up to 81% for the time-splitting formulation and 88% for the nonsplitting formulation. The latter gives better amplitude but significantly broadens the original hill and produces moderate dispersion skirting boundaries

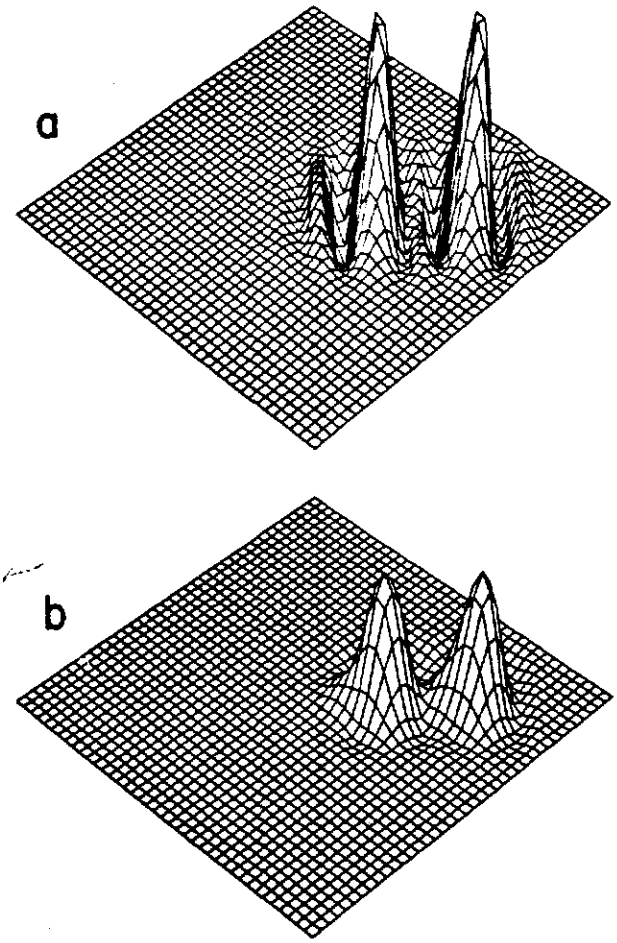

FIG. 7. The results at 3 h in the uniform flow test for (a) scheme L6 using $\Delta t = 360$ s and (b) as in (a) but including the cross-space term.

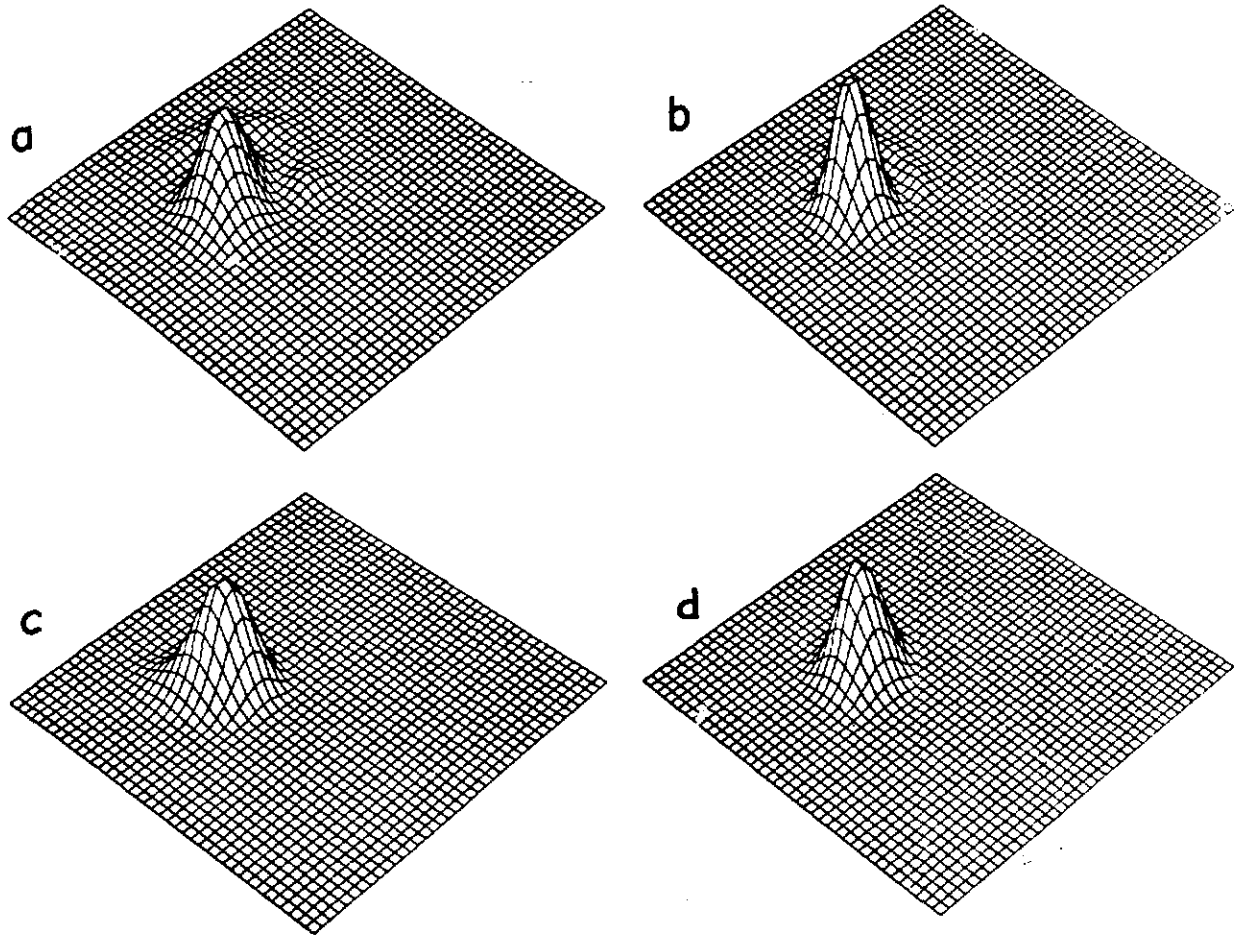

FIG. 8. The results at 12 h (four full rotations) in the rotational flow test for positive-definite scalars. (a) L0 with $\mu = 0.2$, (b) L3, (c) L8M, and (d) L8M with the cross-space term.

(degree D). For positive definite scalars, the slight dispersion given by the time-splitting cubic upstream spline is further reduced for locations where negative values would otherwise occur (thus, degree B^+ is given to distinguish from degree B). The original Crowley schemes L5, L5C, and L5CP are stable but are associated with severe dispersion over the entire domain (degree F). On the other hand, the scheme L5M (the modified Crowley scheme for better amplitude) without the cross-space term is unstable. The stabilities in the central domain for the two schemes L2 and L5M without the cross-space term appear to be gradually contaminated due to the influence of the dispersive waves in a limited domain. In contrast to L2 and L5M, Schlesinger's schemes L6, L6C, and L6CP (the modified Crowley scheme for better phase) are stable, all giving little dispersion (degree A) but poor amplitude preservation (only 31%–32%). L8MP and L8MCP are stable and obtain a final amplitude of about 66%–67% and dispersion of degree A. Schemes L8M and L8MC perform comparably to L8MCP (for positive definite scalars) for the preservation of the hill, except for a major dispersion hole of negative values adjacent to the hill. L8MC gives a less broadened hill after four full rotations as compared to L8M.

The linear results show that adding a numerical filter helps a simple, weakly dissipative advection scheme preserve phase for long-term rotational flow. For scalars without positive definiteness, only scheme L6 yields little dispersion (degree A) without the use of a filter, but the amplitude is preserved only to about one-third of the original value. With the linear filter, all higher-order schemes that otherwise preserve amplitude degrade to some extent. Only time-splitting L3 (a global scheme) can preserve the initial hill satisfactorily without a numerical smoother. A simple finite-difference advection scheme is probably inappropriate for long-term nonlinear advection in rotational flow if both phase and amplitude are to be preserved (Orszag 1971). For rotational flow such as an evolving cyclone, inclusion of the cross-space term will be helpful since the Courant number is strongly confined by the flow itself.

With the cross-space term, the proposed scheme performs comparably to the cubic upstream spline for the rotational flow for somewhat shorter integrations.

4. Linear analyses and nonlinear tests of the modified WKL scheme

As shown in the linear advection tests in the preceding section, the modified WKL scheme is more comparable to the cubic upstream spline than other schemes. Schlesinger's proposed third-order Crowley scheme preserves phase best, but the amplitude is considerably suppressed. The scheme may be desirable in simulations for which phase preservation is important (Schlesinger 1988). It will be shown in this section that the modified WKL scheme can reproduce the features of Crowley-type schemes of third order and can behave similar to Schlesinger's scheme. By virtue of linear analyses for dispersion and dissipation with different ω, it is also possible for the modified WKL scheme to illustrate the limitation of Crowley-type schemes. The features of linear analyses for this scheme and its performance in nonlinear advection are investigated in this section.

a. Linear analyses

The complete 2D modified WKL scheme including the first cross-space term is given by

$$\phi_{i,j}^{n+1} = \phi_{i,j}^{n} - \frac{\alpha}{12}\left(-\phi_{i+2,j}^{n} + 8\phi_{i+1,j}^{n} - 8\phi_{i-1,j}^{n} + \phi_{i-2,j}^{n}\right) + \frac{\alpha^2}{8}\left(\phi_{i+2,j}^{n} - \phi_{i,j}^{n} + \phi_{i-2,j}^{n}\right)$$

$$- \frac{\beta}{12}\left(-\phi_{i,j+2}^{n} + 8\phi_{i,j+1}^{n} - 8\phi_{i,j-1}^{n} + \phi_{i,j-2}^{n}\right) + \frac{\beta^2}{8}\left(\phi_{i,j+2}^{n} - \phi_{i,j}^{n} + \phi_{i,j-2}^{n}\right)$$

$$- \frac{\omega_a}{24}\left(\phi_{i+2,j}^{n} - 4\phi_{i+1,j}^{n} + 6\phi_{i,j}^{n} - 4\phi_{i-1,j}^{n} + \phi_{i-2,j}^{n}\right) - \frac{\omega_b}{24}\left(\phi_{i,j+2}^{n} - 4\phi_{i,j+1}^{n} + 6\phi_{i,j}^{n} - 4\phi_{i,j-1}^{n} + \phi_{i,j-2}^{n}\right)$$

$$+ \frac{\alpha\beta C_s}{4}\left(\phi_{i+1,j+1}^{n} - \phi_{i-1,j+1}^{n} - \phi_{i+1,j-1}^{n} + \phi_{i-1,j-1}^{n}\right), \quad (17)$$

where the constant C_s is unity or zero for the inclusion or exclusion of the cross-space term, respectively, and ω_a and ω_b are the two free controlling parameters used in the respective x and y directions. For the choice of ω, we use

$$\omega_a = 4\alpha^2 \text{ and } \omega_b = 4\beta^2, \text{ for minimum dissipation,}$$

$$\omega_a = 0.8(4\alpha^2 + 1) \text{ and } \omega_b = 0.8(4\beta^2 + 1),$$

$$\text{for minimum dispersion.} \quad (18)$$

A Fourier component of the solution for the finite-difference advection equation may be expressed as

$$\phi_{i,j}^{n} = \phi_0 \exp[\sqrt{-1}(ki\Delta x + lj\Delta y + \omega n\Delta t)]$$

$$= \phi_0 \exp[\sqrt{-1}(ki\Delta x + lj\Delta y)]G^n, \quad (19)$$

where ϕ_0 is the initial amplitude, k and l are wavenumbers in the x and y directions, respectively, and ω is frequency, and

$$G = \exp(\sqrt{-1}\,\omega\Delta t), \quad (20)$$

where G is a complex constant termed the amplification factor that indicates stability at each time step. For a single component, a time integration of an advection scalar is considered to be stable if $|G| \leq 1$ and unstable otherwise. Separating the wave frequency and the amplification factor into real and imaginary parts,

TABLE 1. The results after four full rotations for different schemes in the rotational flow test. Characters in labels for each run: C, the cross-space term is used; P, positive-definite scalar is assumed. The final maximum amplitude is relative to the initial maximum amplitude.

Experiment	Maximum amplitude (%)	Degrees of dispersion*
L0 (μ = 0.05)	63	F
L0 (μ = 0.25)	53	E
L0 (μ = 0.05; S = 0.125, −0.125)	51	C
L0 (μ = 0.25; S = 0.125, − 0.125)	43	B
L0P (μ = 0.20)	59	B
L2, L2C, L2CP	174, 59, 57	C
L3 (nonsplitting)	88	D
L3 (splitting)	81	B
L3P (splitting)	80	B+
L5, L5C, L5CP	27, 29, 40	F
L5M, L5MC	∞**, 63	E
L5MC (S = 0.125, −0.125)	43	B
L6, L6C, L6CP	32, 31, 32	A
L8MP, L8MCP	67, 66	A

* Degrees of dispersion are: A, almost dispersion-free everywhere; B, slight dispersion near the hill; C, moderate dispersion near the hill; D, moderate dispersion near the hill and boundaries; E severe dispersion near the hill; F, severe dispersion everywhere.

** The scheme L5M without the cross-space term had such severe instability that numerical overflow occurred before four full rotations.

$$\begin{cases} \omega = \omega_R + i\omega_I, \\ G = G_R + iG_I, \end{cases} \tag{21}$$

we obtain for this scheme

$$G_R = 1 + \left(\frac{\omega_a}{3}\right)\cos(\theta_x) + \left(\frac{\alpha^2}{4} - \frac{\omega_a}{12}\right)\cos(2\theta_x) + \left(\frac{\omega_b}{3}\right)\cos(\theta_y) + \left(\frac{\beta^2}{4} - \frac{\omega_b}{12}\right)\cos(2\theta_y) - \frac{\alpha^2+\beta^2}{4} - \frac{\omega_a+\omega_b}{4} - \alpha\beta C_s \sin(\theta_x)\sin(\theta_y),$$

$$G_I = -\frac{4\alpha}{3}\sin(\theta_x) + \frac{\alpha}{6}\sin(2\theta_x) - \frac{4\beta}{3}\sin(\theta_y) + \frac{\beta}{6}\sin(2\theta_y) \tag{22}$$

where $\theta_x = k\Delta x$ and $\theta_y = l\Delta y$. The absolute value of G, the eigenvalue of Eq. (17), is given by

$$\lambda = (G_R^2 + G_I^2)^{1/2}, \tag{23}$$

and the relative phase error is determined following Schlesinger (1985) as

$$\epsilon_\phi = \frac{-\tan^{-1}(G_I/G_R)}{\alpha\theta_x + \beta\theta_y} - 1. \tag{24}$$

Negative (positive) values of ϵ_ϕ indicate lagging (leading) phase error. Note that the minus sign associated with the cross-space term in (22) indicates that this term always increases numerical stability, since $0 \leq \theta_x \leq \pi$ and $0 \leq \theta_y \leq \pi$ for all resolvable wavelengths. This increase in stability reaches a maximum for 4Δ ($\Delta x = \Delta y = \Delta$) waves. Thus, the cross-space term will stabilize shorter waves in particular.

Figure 9 shows contour plots of λ as functions of α and β for a given wavelength of $n\Delta x = n\Delta y = n\Delta$ and ω (the cross-space term has been included). Contours are plotted only for wavelengths of 6Δ ($n = 6$) and 10Δ ($n = 10$), since λ for 2Δ wavelength is much smaller than unity. The values of λ for 4Δ wavelength are also important for a numerical scheme, but the contour plot for 6Δ wavelength was selected in order to compare the results with those of Schlesinger (1985). Using $\omega = \omega_1$, this scheme has slight instability for small Courant numbers. Instability is maximized at the diagonal line ($\alpha = \beta$). Indeed, the maximum stable diagonal Courant number is zero for $\omega = \omega_1$. However, the maximum stable value for each directional Courant number is much larger, indicating the scheme to be more favorable for 1D advection. The results are also found in the original second-order Crowley scheme for which 1D advection is stable with α less than unity but 2D advection is unstable with any permutation of α and β according to linear analyses (Smolarkiewicz 1982). With $\omega = 2\omega_1$, the maximum stable diagonal Courant number increases for both 6Δ and 10Δ wavelengths. As ω increases again (e.g., $\omega = \omega_2$), the stability increases further. For the amplification factor λ, the proposed scheme will essentially resemble Schlesinger's scheme (Fig. 1 in his paper) if ω is chosen close to ω_2. Using $\omega = \omega_2$, this scheme has moderate dissipation for low diagonal Courant numbers. In the UL test, the performances of the quadratic upstream interpolation and Schlesinger's scheme are near equivalent to that of the proposed scheme with $\omega = 3\omega_1$ and $\omega = \omega_2$, respectively.

Figure 10 shows the contours of ϵ_ϕ for 6Δ and 10Δ wavelengths. It is seen that the phase errors for any of the three options, $\omega = \omega_1$, $\omega = 2\omega_1$, and $\omega = \omega_2$, are much smaller (only several percent) than those (larger than several tens of percent) for the original Crowley scheme and the second-order leapfrog scheme (see Haltiner and Williams 1980). For these two wavelengths (6Δ and 10Δ), phase errors in the low Courant number regime are 2% or less despite different values of ω. Since the scheme is fourth-order accurate only in the case of $\omega = \omega_1$, the features of the associated phase error are particularly interesting. We see that there exists a curve of zero phase error for a Courant number of approximately 0.41 for this case. Similar results also appear in the case of $\omega = 2\omega_1$, but the curve of zero phase error is shifted to smaller Courant numbers. Both the cases give lagging phase (negative ϵ_ϕ) for lower Courant numbers consistent with the linear test results shown before. Surprisingly, a line of zero phase error does not exist for low Courant numbers when $\omega = \omega_2$ (but the phase error is still small).

Figure 11 shows λ and ϵ_ϕ as functions of wavenumbers n given $\alpha = \beta = 0.1$ and $\alpha = \beta = 0.2$. As can be seen, there is almost no long-wave phase and amplitude misrepresentation for the three options, $\omega = \omega_1$, $\omega = 2\omega_1$, and $\omega = \omega_2$. Slight short-wave instability is found for $\omega = \omega_1$ and no instability for the other two cases. The case of $\omega = \omega_2$ for minimum dispersion gives nearly the same magnitudes of dispersion as the other two cases, but the short-wave phase error changes from lagging to leading.

Although the minimum dispersion scheme ($\omega = \omega_2$) does not show better phase preservation than the minimum dissipation scheme (with $\omega = \omega_1$), the phase preservation of this scheme is actually better in tests and is almost as free of dispersion (Fig. 10) as the first-order upstream scheme discussed by Pielke (1984). The Fourier component analyses of the upstream scheme indicate the scheme to have strong dispersion. A similar situation is also found in the leapfrog scheme, which is theoretically neutral (i.e., dissipation-free). It has been shown in the preceding section that both the second-order and the fourth-order leapfrog schemes, however, do not preserve all of the initial amplitudes because of the associated dispersive errors. It is thus

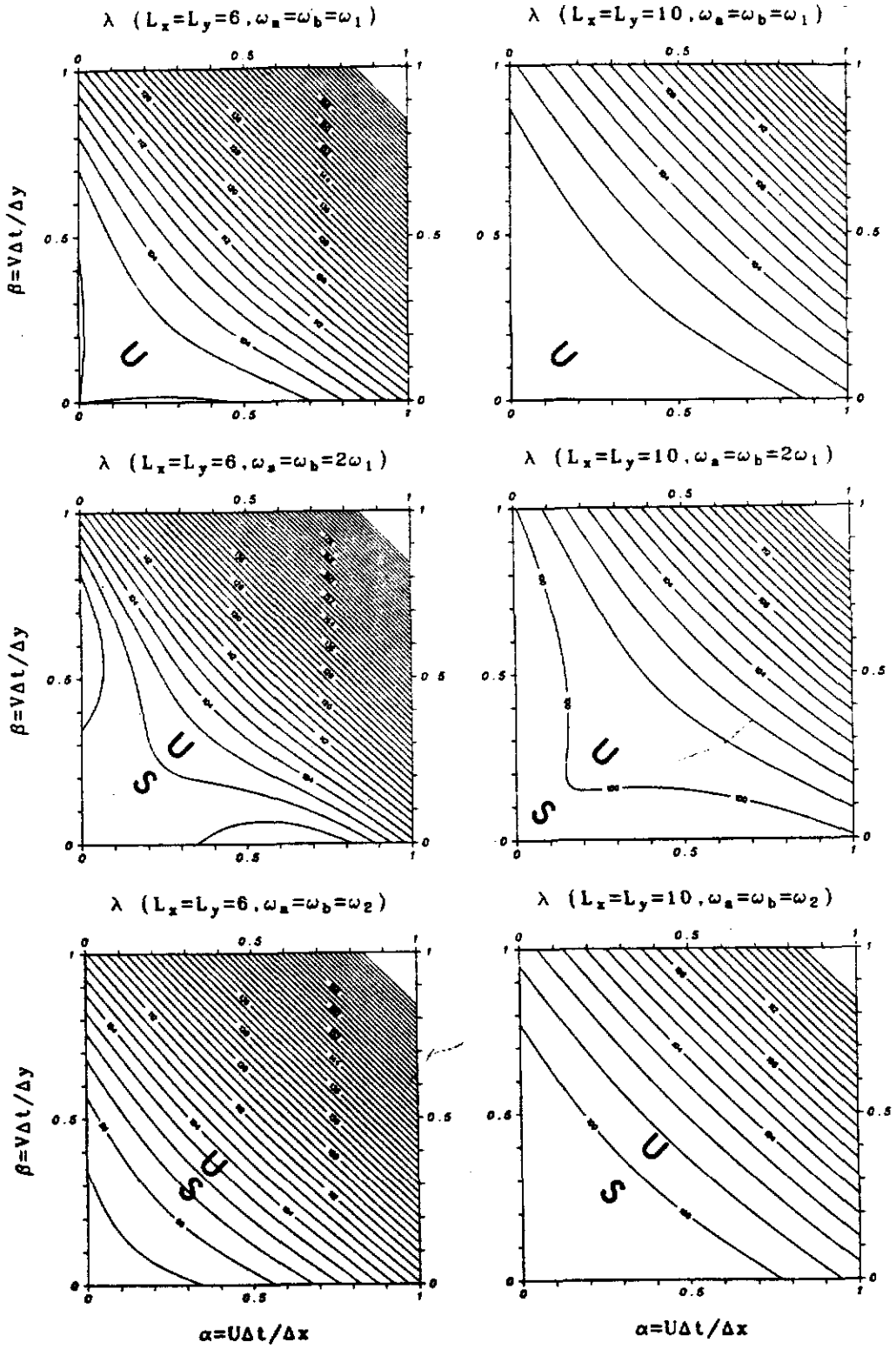

FIG. 9. Contours of 6Δ and 10Δ wave amplification factors as functions of directional Courant numbers, α and β, for the proposed modified WKL scheme (including the first cross-space term) with the free parameter $\omega = \omega_1$, $2\omega_1$, and ω_2. Characters S and U indicate stable and unstable regions, respectively, and contour intervals for 6Δ and 10Δ waves are 2 units and 1 unit, respectively. A scaling by 100 for λ is used for all panels.

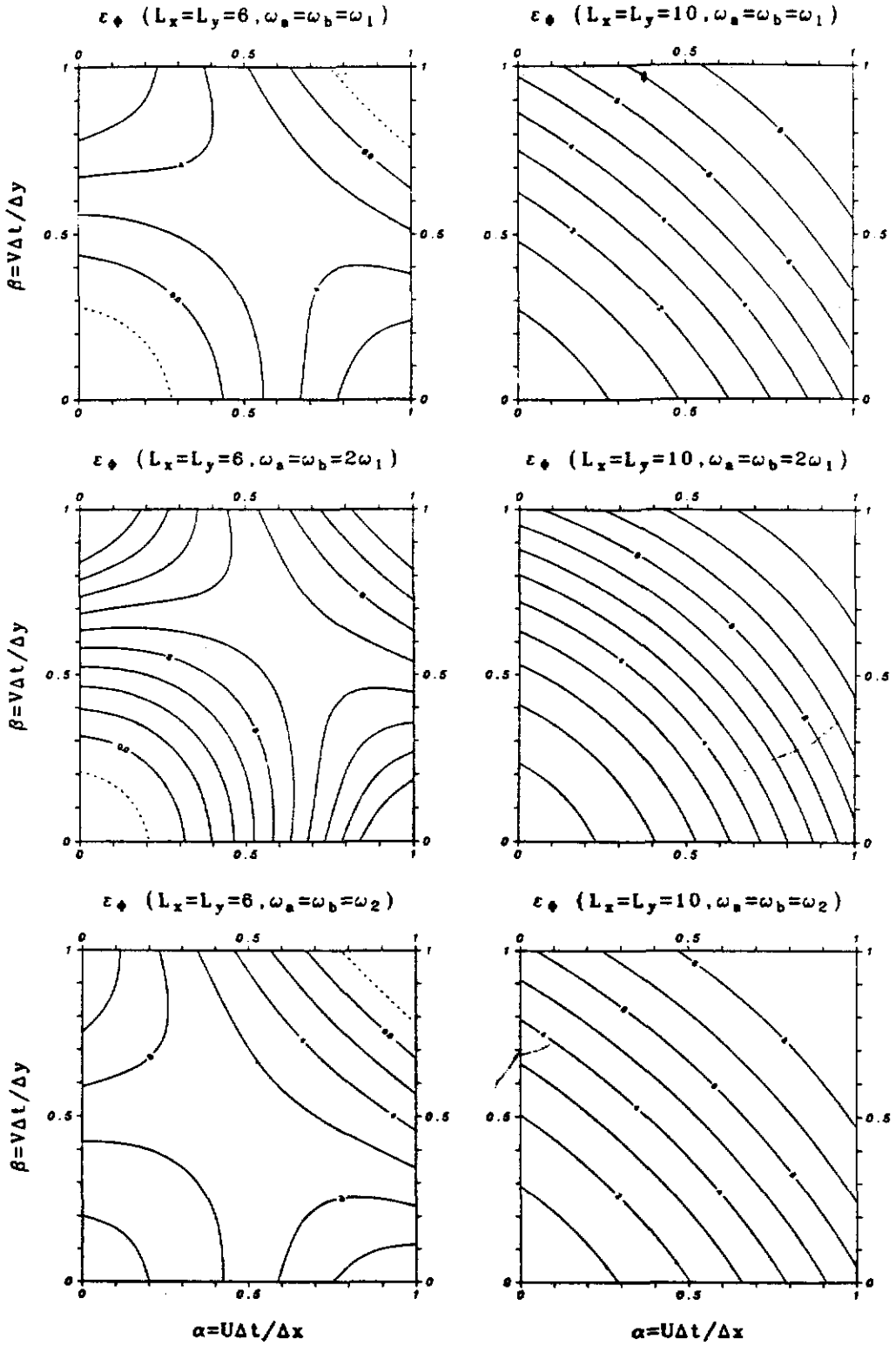

FIG. 10. As in Fig. 9 except for the phase errors. Negative values represent lagging phases and positive values leading phases. Contour intervals are the same as in Fig. 9. A factor of 100 for ϵ_ϕ is used for all panels.

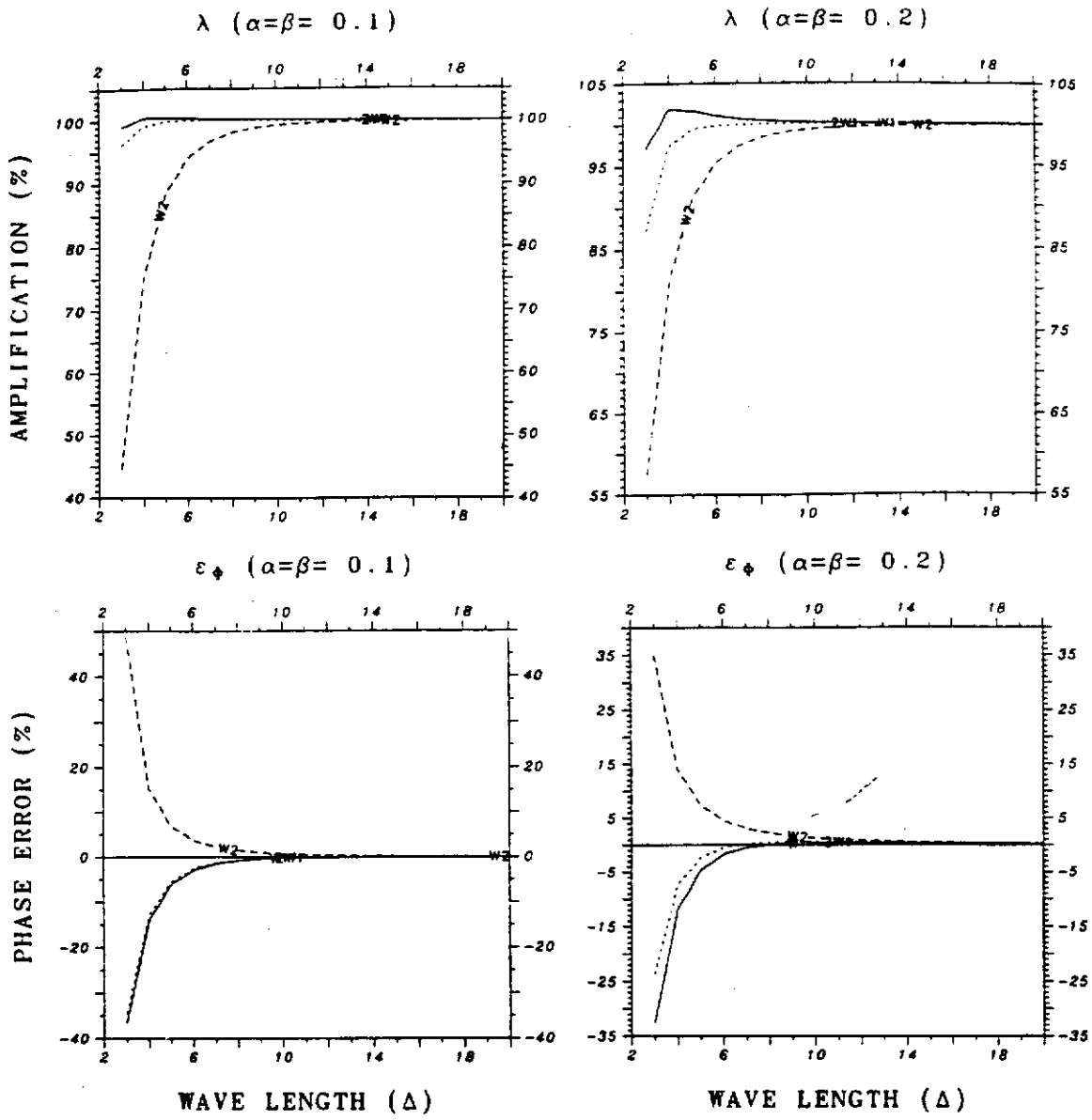

FIG. 11. Amplification factors and phase errors (scaled by 100) as functions of wavelength ($n\Delta$) at $\alpha = \beta = 0.1$ and 0.2 for $\omega = \omega_1$ (solid line), $2\omega_1$ (dotted line), and ω_2 (dashed line) in the modified WKL scheme (includin g the first cross-space term).

obvious that one single Fourier component cannot totally describe the global features of an advection scheme. Although both the initial and advective phases of a scalar field are nondispersive, dispersive phase error during numerical integration results in the misrepresentation of the total amplitude despite the influence of boundary conditions. Slight unstable modes ($\lambda > 1$) may be offset by other stable modes ($\lambda < 1$) and amplification is thus slowed down or even eliminated.

With the option of $\omega = \omega_1$ for minimum dissipation, the modified WKL scheme shows slight instability for shorter waves for low Courant numbers. Figure 12a shows the maximum diagonal Courant number ($\alpha = \beta$) for $\lambda < 1.01$. (Due to the tolerance in global instability as discussed above, $\lambda = 1.01$ is arbitrarily chosen as a threshold of instability.) The scheme using $\omega = \omega_1$ gives relatively low maximum stable Courant numbers for short waves (approximately 4Δ). On the other hand, including the cross-space term greatly increases the maximum stable Courant number for all wavelengths except for 2Δ waves, as revealed by (22). With the cross-space term, the schemes using $\omega = 2\omega_1$ and $\omega = \omega_2$ have almost the same maximum diagonal Courant number for $\lambda < 1.01$.

Figure 12b shows the maximum λ for the range of 2Δ–40Δ waves for a given diagonal Courant number

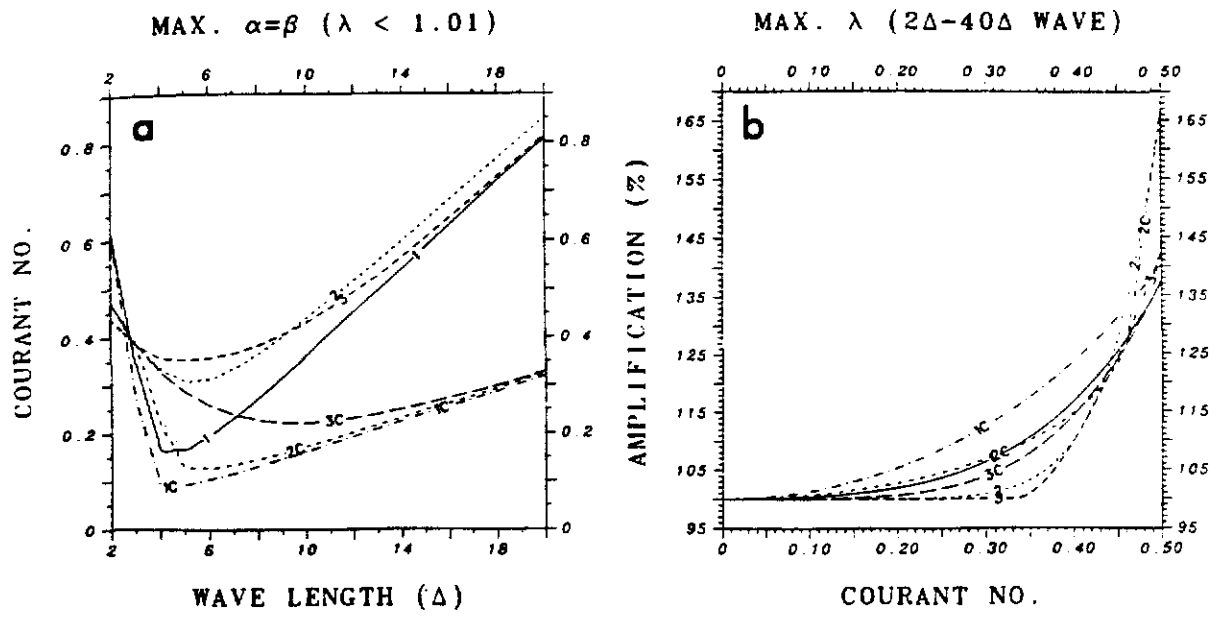

FIG. 12. (a) Maximum diagonal Courant number ($\alpha = \beta$) as a function of wavelength (Δ) for amplification factor < 1.01 in the modified WKL scheme (including the first cross-space term). Specifications for the number symbols plotted in lines are: 1 for ω_1, 2 for $2\omega_1$ and 3 for ω_2; Character C following the number in lines indicates that the cross-space term is not included in that case. (b) Maximum amplification factor (scaled by 100) as a function of diagonal Courant number ($\alpha = \beta$). The maximum value is determined numerically for wavelengths between 2Δ and 40Δ. The symbols plotted along the curves are the same as in (a).

($\alpha = \beta$). It is obvious from this figure that the cross-space term can decrease the slope of amplification factor and thus increase the Courant number at $\lambda = 1$. With the cross-space term, the scheme is absolutely stable if the diagonal Courant number is less than 0.22 for $\omega = 2\omega_1$ and less than 0.33 for $\omega = \omega_2$. For $\omega = \omega_1$, the maximum stable Courant number is very small, and it is almost zero if there is no tolerance allowed in amplification. It is obvious that decreased dissipation for the Crowley-type schemes tends to diminish the maximum stable Courant number. Although higher-order Crowley-type schemes give better phase accuracy, the associated maximum stable Courant number will be smaller than at second order. This result is also found for the second-order and fourth-order leapfrog schemes (Haltiner and Williams 1980).

It is difficult to determine the best value for the controlling parameter ω in the modified WKL scheme with selective control (L8M) for nonlinear advection of fields that are not positive definite. For example, dispersion of negative values cannot be avoided if these values are not reset to zero. A similar problem also exists in flux-corrected transport schemes (Boris and Book 1976; Zalesak 1979) in which a hybrid form consisting of a low-order and a high-order scheme is used (the low-order scheme is applied for stronger diffusion). A region that needs stronger diffusion will not be easy to define except for positive definite scalars. Peyret and Taylor (1983) thus argued that although the flux-corrected transport method is simple in principle, there is no clear "best" general approach for various flow problems. The strong dependence on the characteristics of the scalars (or flow) is the major disadvantage of the modified WKL scheme when applied to advecting fields without positive definiteness.

b. *Nonlinear advection tests*

It is desirable to test the modified WKL scheme in 2D and 3D nonlinear advection for its applicability to weather forecast problems. The reliability of the scheme in nonlinear advection will be examined using a hydrostatic and anelastic primitive equation model (Huang 1990) in a terrain-following coordinate system. Shapiro's linear filter is used to control numerical aliasing errors in the nonlinear simulation. Since ω is derived at uniform grid intervals for the modified WKL scheme, it may not be appropriate to apply the scheme for vertical advection in a stretched grid mesh used in the nonlinear model. For both 2D and 3D simulations, the scheme tested is thus applied only to the horizontal, while the quadratic upstream interpolation is used in the vertical.

The 2D nonlinear advection test is chosen such that the exact wave phase and magnitude can be determined theoretically for comparison. The simulation of 2D hydrostatic mountain waves may satisfy the above consideration since they have been extensively studied numerically and theoretically by many investigators (Smith 1979; Mahrer and Pielke 1978; Klemp and Lilly 1978; Klemp and Durran 1983). Considerable changes are required in the model codes when the three-time-

level leapfrog scheme is incorporated. Hence, only the results given by the modified WKL scheme and the other two-time-level schemes including the cubic upstream spline will be directly compared.

A uniform wind of $U = 20$ m s^{-1} and $V = 0$ m s^{-1} and a constant vertical gradient of 4°C km^{-1} for the potential temperature are specified as the initial conditions for use in the 2D nonlinear flow test. In the model, the potential temperature is a positive definite scalar because no perturbation part is partitioned in addition to the basic profile. A free-slip condition is assumed for the wind at the lower boundary. The Coriolis force has been omitted in the simulation. The horizontal and vertical grid intervals are $\Delta x = 7.5$ km and $\Delta z = 500$ m, respectively, with a time step Δt of 40 s. There are 30 and 25 grid points in the respective x and z directions of the model domain in which a bell-shaped mountain of 1-km height is specified at the center (grid number 15 in the x direction). Half-width of the mountain is 15 km (two horizontal grid intervals). A radiation upper boundary condition (Klemp and Durran 1983) is used to determine the upper perturbation pressure. This radiation condition has been shown to be important for correctly simulating mountain waves and could be used instead of an absorbing layer above the physical domain height (12 km in this case). The mountain is included at the first time step. This means that the mountain is lifted instantaneously to the actual height once the model integration starts. Although the initial fields are balanced, the solution will not be hampered by the initialization as the flow approaches a steady state.

Figure 13 shows the quasi-steady state results at 12 h for the quadratic upstream interpolation (L2), the cubic upstream spline (L3), the second-order Crowley scheme (L5), and the modified WKL scheme (L8) with $\omega = 2.5\ \omega_1$. Dispersion due to advection would not cause negative potential temperature because the typical magnitude of the potential temperature is around 300 K. Hence, selective control for L8M would not be invoked for this case. Note that the cross-space term with respect to the x and z directions was not included. As can be seen, mountain waves tilt upstream and the maximum amplitudes of the waves are about the same for all the schemes. The dominant nonlinear mountain waves in the forced circulation are not attenuated significantly for all the schemes even though the linear filter is used. To obtain reasonable amplitudes of nonlinear mountain waves, a second-order scheme such as L5 seems to be sufficient (the wind disturbances in fact are slightly stronger than those given by L3 and L8). It can be found, however, that scheme L5 gives a low-level perturbation center in the wind field about one grid interval farther upstream than the higher-order schemes, which appear to better preserve the upper-level phase of the wind. The corresponding linear solution (assuming small perturbation amplitude) indicates that the low-level perturbation center of the buoyancy-dominant flow on this scale should be directly above the mountaintop as was obtained by the three higher-order schemes (Smith 1979; Durran and Klemp 1983).

For all the higher-order schemes, the mountain waves show a trough at 5.5–6 km and a ridge at 11–12 km as seen in the potential temperature field. The vertical wavelength is thus about 11–12 km, consistent with the theoretical value (11.5 km) of $2\pi U/N$ where N is the atmospheric stability frequency (Smith 1979). Note that due to the nonlinear lower boundary condition in association with the mountain of 1-km height, the vertical mountain wavelength estimated by the perturbation centers in the wind field is slightly different from that by the potential temperature field.

Using $\omega = \omega_1$ for least dissipation, the modified WKL scheme (L8) gives nearly the same maximum wind speed and potential temperature field (not shown), but the upper-level wind field is slightly distorted as compared to that using $\omega = 2.5\omega_1$. The dispersion conditions associated with least dissipation depend on the chosen Courant number, as discussed before (see Fig. 10). For the nonlinear flow, the total phase dispersion of all wave modes is complex. As a result, the use of $2\omega_1 \leqslant \omega \leqslant 3\omega_1$ is considered to be more appropriate for general simulation. This choice will make the performance of the modified WKL scheme closer to that of the quadratic upstream interpolation, a compromise between Schlesinger's scheme and the original Crowley advection scheme. There is no best choice of ω for obtaining both the best phase and the best amplitude in the nonlinear case. The nonlinear simulations also show the limitation of the Crowley-type schemes for which better amplitude preservation results in larger dispersion. But, the dispersion given by fourth-order schemes is generally smaller than for second-order schemes as seen in this test. The modified WKL scheme without the use of least dissipation correctly simulates the mountain waves and is comparable to the cubic upstream spline for this case and the fourth-order leapfrog scheme for similar conditions (Klemp and Durran 1983).

Since the ultimate test for an advection scheme is its 3D performance, 3D numerical experiments were also conducted using the same model. The terrain is bell-shaped and symmetric to the central grid of the lowest model layer. The model domain has 30 × 30 grid points in the horizontal. Initially, $U_g = V_g = U = V = 10$ m s^{-1} where U_g and V_g are the east–west and north–south geostrophic wind components, respectively, and a constant vertical gradient of 4°C km^{-1} up to 12-km height is specified for the potential temperature. Turbulent transfers in the planetary boundary layer are determined using a second-order closure scheme in which two prognostic equations, one for turbulent kinetic energy and the other for turbulent energy dissipation, are employed. A no-slip condition is used for the wind on the ground above which a neu-

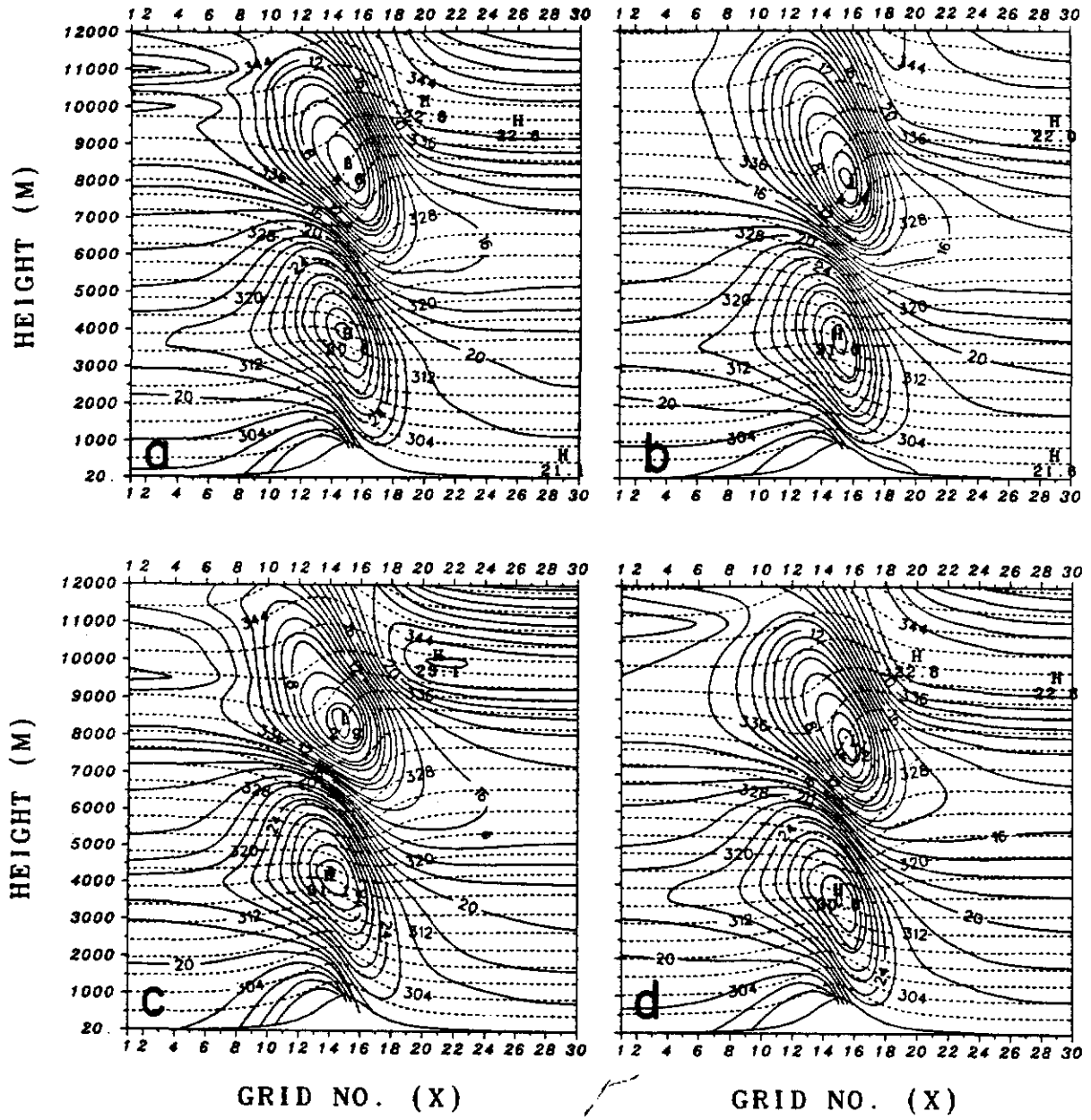

FIG. 13. The east–west wind component (solid lines) and potential temperature (dashed lines) at 12 h in the 2D nonlinear mountain wave simulation for (a) the quadratic upstream interpolation, (b) the cubic upstream spline, (c) the Crowley scheme, and (d) the modified WKL scheme L8 with $\omega = 2.5\omega_1$ (see text for ω_1). Contour intervals for U and θ in each panel are 1 m s^{-1} and 1 K, respectively.

tral layer of 50-m thickness is assumed to keep the boundary condition simple. In the 3D case, the cross-space term related to the x and y directions is included in the modified WKL scheme with the selective control on dispersion for the positive-definite prognostic variables such as water vapor, cloud water, rainwater, turbulent kinetic energy, and turbulent dissipation. For other prognostic fields such as wind velocities and potential temperature, $\omega = 2.5\omega_1$ (i.e., $\omega_a = 10\alpha^2$ and $\omega_b = 10\beta^2$ in the 2D formulation). The total integration time for the 3D case is 8 h, with a time step of 30 s. A description of the numerical model is given in detail by Huang (1990).

Figure 14 shows the results for vertical velocity and cloud water at a height of 250 m for the modified WKL scheme and the cubic upstream spline. Cloud water is maximum at this height with the maximum loading over the peak and a diluted cloud band downstream. The downstream extension of the cloudy zone is caused by the flow convergence downwind of the hill. It can

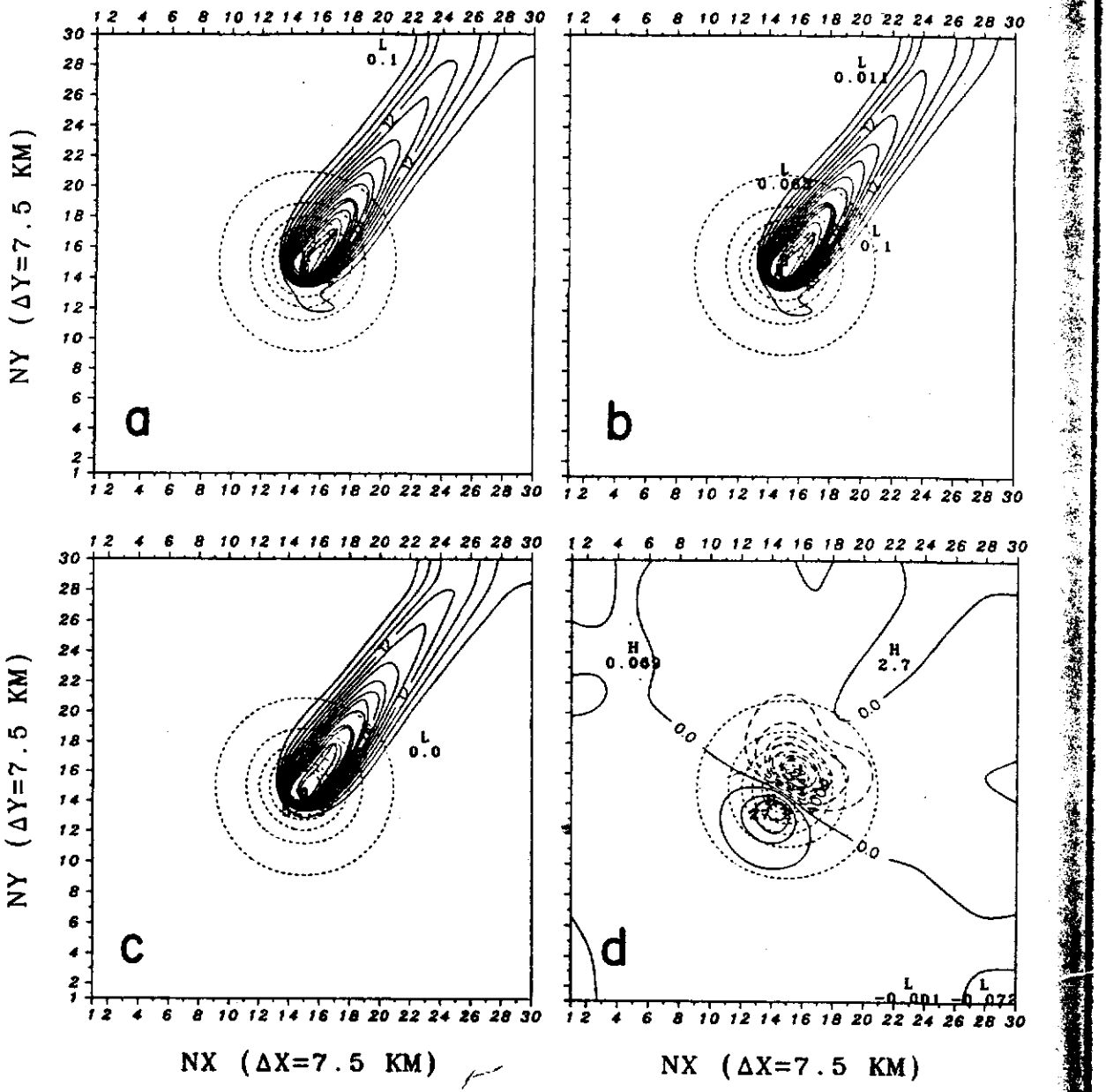

FIG. 14. The results in the layer of 250-m height at 8 h for the 3D flow over an isolated hill of 1-km height (shorter dashed contour lines with an interval of 100 m). Initially, relative humidity is 80% uniformly in the vertical and no cloud water exists. (a) cloud water q_c for the nonsplitting cubic upstream spline, (b) as in (a) but for time-splitting form, (c) as in (a) but for the modified WKL scheme, and (d) as in (c) but for vertical velocity. Contour intervals for W and q_c are 5 cm s^{-1} and 0.03 g kg^{-1}, respectively.

be found that the configuration and maximum water loading of the clouds (about 0.51–0.52 g kg^{-1}) for the two schemes are approximately the same, although the maximum vertical motions for the cubic upstream spline are slightly larger than those for the modified WKL scheme (with the option of moderate dissipation for non-positive-definite scalars). The 3D solution of the flow with the cloud effects cannot be obtained without recourse to numerical simulation. As a result, there is slight dispersion of cloud water upstream of the cloud core for both the splitting and nonsplitting forms of the cubic upstream spline. This feature does not appear in the results for the second-order Crowley scheme (not shown) and the modified WKL scheme. This upstream dispersion of cloud water is not physically plausible. The modified WKL scheme therefore appears to be more appropriate for the nonlinear advection of positive-definite scalars than the cubic upstream spline at least for this case.

Table 2 gives an outline of some reference data, such

TABLE 2. Comparisons of 3D results and the computer times for the schemes tested for nonlinear flow.

Experiment	W_{max}	W_{min}	q_c	(i, j)	CPU (h)
L3 (nonsplitting)	30.1	−59.2	0.512	(15, 15)	61.6
L3 (splitting)	29.4	−58.3	0.508	(15, 15)	61.6
L5	30.3	−52.9	0.612	(15, 14)	43.3
L8M ($\omega = \omega_1$)	30.7	−60.2	0.488	(15, 15)	44.9
L8M ($\omega = 2.5\ \omega_1$)	27.2	−53.9	0.523	(15, 14)	44.6

W_{max} and W_{min} are the maximum and minimum vertical velocities (cm s^{-1}), respectively, in the layer of 250-m height where cloud water q_c (g kg^{-1}) is maximum. The grid indices (i, j) indicate the location of the maximum q_c. The CPU time also involves the computations of cloud microphysics and subgrid turbulent transfer. The advection schemes were applied only in the horizontal, in combination with the quadratic upstream interpolation in the vertical. All computations were accomplished on the microcomputer VAX 3100.

as simulated system intensities and computer times for the schemes tested in the 3D case. All the schemes predict the same height (z = 250 m over the ground) and nearly the same location for maximum cloud-water loading. With the option of least dissipation ($\omega = \omega_1$), the modified WKL scheme (L8M) gives slightly stronger vertical motions at a height of 250 m than those obtained using $\omega = 2.5\omega_1$ and the cubic upstream spline (L3), but the associated maximum cloud water is smaller. On the other hand, the Crowley scheme (L5) yields nearly the same maximum upward motion ahead of the hill, but the cloud water is considerably larger (approximately 0.1 g kg^{-1} more) than those given by other schemes. The cloudy zones for all the schemes are similar in distribution and width, however, the axis of the cloudy zone shifts slightly to the southeast for the WKL scheme with $\omega = \omega_1$ and to the northwest for the Crowley scheme (not shown), as compared to the WKL scheme with $\omega = 2.5\omega_1$ and the cubic upstream spline. It is interesting to note that the Crowley scheme preserves phase and amplitude fairly well in the 3D rather than 2D case. This is partly due to the fact that the magnitude of the forced mountain waves in the 3D flow is considerably smaller than that in the 2D flow. Another reason is that the structures resolved by the second-order and higher-order schemes are more similar at low levels than at higher levels. This was also seen in the 2D case results.

Finally, computation time is a factor to be considered. In the 2D linear flow tests, computer time for the cubic upstream spline is 2–3 times larger than that for the modified WKL scheme. However, the total CPU time in the 3D run (see Table 2) using the cubic upstream spline is only modestly larger than those using other schemes. This is because computations of turbulent transfer and cloud microphysics are also time-consuming. Use of the cubic upstream spline is thus desirable in some simulations involving complex physics.

5. Concluding remarks

In this study, we tested some finite-difference advection schemes commonly used in meteorological numerical models and also examined the effects of the associated numerical components such as numerical smoothing and the cross-space terms. In light of the poorer amplitude preservation of existing Crowley-type advection schemes in comparison with the fourth-order leapfrog scheme, we propose a fourth-order Crowley-type scheme which is based on the multistep Warming–Kutler–Lomax (WKL) scheme. The modified WKL scheme has the features of two-time levels and one-step computation as in the original second-order Crowley scheme.

One of the advantages of the proposed scheme over other Crowley-type schemes is that it uses a free parameter to control dissipation and dispersion. Because of its selective control on dispersion, the scheme is suitable for the advection of positive-definite scalars such as moisture. Besides, the scheme is shown to be theoretically a generalization of third-order Crowley-type schemes, because if the free parameter is suitably adjusted the results can closely reproduce the beneficial features of those schemes. There remains, however, a significant limitation on the Crowley-type schemes for which better amplitude preservation would require a smaller integration time step since diffusion is required for numerical stability. Schemes with better phase accuracy can use larger time steps, but they inevitably preserve amplitude worse.

The results given by the modified WKL scheme in linear advection for scalars without definite positiveness are near identical to those of the fourth-order leapfrog scheme with suitable time smoothing. For positive-definite scalars, this scheme performs better than the fourth-order leapfrog scheme because of the selective control on dispersion, and it is more comparable to the cubic upstream spline. Inclusion of the cross-space term in the Crowley-type schemes helps stabilize the long-term rotational flow but does not improve the results for time steps too small to cause overshooting in the long run. Combination of a linear space filter for a simpler amplitude-preserving scheme other than the cubic upstream spline is necessary in order to obtain reasonably correct phase in long-term rotational flow.

When applied to the simulation of 2D nonlinear mountain waves, the modified WKL scheme yields satisfactory results compared to those of the cubic upstream spline and mountain wave theory. For the sim-

ulation of 3D flow over an isolated hill, the scheme performs comparably to the cubic upstream spline, indicating its reliability in representing multidimensional advection. The proposed scheme can thus be used as an option in a numerical model to save computer resources because more computer memory is required for the leapfrog scheme and more computer time is required for the cubic upstream spline. The modified WKL scheme has been used to simulate the 3D moist flow over the Gulf Stream region and steep mountains in Taiwan (Huang 1990), and the results are encouraging.

Acknowledgments. The authors wish to thank the reviewers for helpful suggestions. This work was supported by the Division of Atmospheric Sciences, National Science Foundation under Grant ATM-88-01650.

REFERENCES

Anderson, D. A., and B. Fattahi, 1974: A comparison of numerical solutions of the advective equation. *J. Atmos. Sci.*, **31**, 1500–1506.

——, J. C. Tannehill and R. H. Pletcher, 1984: *Computational Fluid Mechanics and Heat Transfer*. McGraw-Hill, 599 pp.

Boris, J. P., and D. L. Book, 1976: Flux-corrected transport III: Minimal-error FCT algorithms. *J. Comput. Phys.*, **20**, 397–431.

Crowley, W. P., 1968: Numerical advection experiments. *Mon. Wea. Rev.*, **96**, 1–11.

Durran, D. R., and J. B. Klemp, 1983: A compressible model for the simulation of moist mountain waves. *Mon. Wea. Rev.*, **111**, 2341–2361.

Fromm, J. E., 1969: Practical investigation of convective difference approximations of reduced dispersion. *Phys. Fluids*, **Suppl. II**, 3–12.

Haltiner, G. J., and R. T. Williams, 1980: *Numerical Prediction and Dynamic Meteorology*. 2d ed. Wiley, 477 pp.

Huang, C. Y., 1990: A mesoscale planetary boundary layer numerical model for simulations of topographically induced circulations. Ph.D. dissertation, North Carolina State University, Raleigh, 253 pp.

Klemp, J. B., and D. K. Lilly, 1978: Numerical simulation of hydrostatic mountain waves. *J. Atmos. Sci.*, **35**, 78–107.

——, and D. R. Durran, 1983: An upper-boundary condition permitting internal gravity wave radiation in numerical mesoscale models. *Mon. Wea. Rev.*, **111**, 430–444.

Lax, P. D., and B. Wendroff, 1960: Systems of conservation laws. *Comm. Pure Appl. Math.*, **13**, 217–237.

Leith, C. E., 1965: Numerical simulation of the earth's atmosphere. *Methods Comput. Phys.*, **4**, 1–28.

Leonard, B. P., 1979: A stable and accurate convective modeling procedure based on quadratic upstream interpolation. *Comput. Methods Appl. Mech. Eng.*, **19**, 59–98.

Long, P. E., Jr., and D. W. Pepper, 1976: A comparison of six numerical schemes for calculating the advection of atmospheric pollution. Preprints, *Symposium on Atmospheric Turbulence, Diffusion, and Air Quality*, Raleigh, Amer. Meteor. Soc., 181–187.

Mahrer, Y., and R. A. Pielke, 1978: A test of an upstream spline interpolation technique for the advective terms in a numerical mesoscale model. *Mon. Wea. Rev.*, **106**, 818–830.

Mesinger, F., and A. Arakawa, 1976: Numerical methods used in atmospheric models *GARP Publ. Ser.*, **17**, 1–64.

Miller, M. J., and A. J. Thorpe, 1981: Radiation conditions for the lateral boundaries of limited area numerical models. *Quart. J. Roy. Meteor. Soc.*, **107**, 615–628.

Orszag, S. A., 1971: Numerical simulation of incompressible flows with simple boundaries: Accuracy. *J. Fluid Mech.*, **49**, 75–112.

Petschek, A. G., and L. D. Libersky, 1975: Stability, accuracy, and improvement of Crowley advection schemes. *Mon. Wea. Rev.*, **103**, 1104–1109.

Peyret, R., and T. D. Taylor, 1983: *Computational Method for Fluid Flow*. Springer, 358 pp.

Pielke, R. A., 1984: *Mesoscale Meteorological Modeling*. Academic Press, 612 pp.

Purnell, D. K., 1976: Solution of the advective equation by upstream interpolation with a cubic spline. *Mon. Wea. Rev.*, **104**, 42–48.

Robert, A. J., 1966: The integration of a low spectral form of the primitive meteorological equations. *J. Meteor. Soc. Japan*, **44**, 237–245.

Schlesinger, R. E., 1985: Effects of upstream-biased third-order space correction terms on multidimensional Crowley advection schemes. *Mon. Wea. Rev.*, **113**, 1109–1130.

——, 1988: Effects of stratospheric lapse rate on thunderstorm cloud-top structure in a three-dimensional numerical simulation. Part I: Some basic results of comparative experiments. *J. Atmos. Sci.*, **45**, 1555–1570.

Shapiro, R., 1971: The use of linear filtering as a parameterization of atmospheric diffusion. *J. Atmos. Sci.*, **28**, 523–531.

Smith, R. B., 1979: The influence of mountains on the atmosphere. *Adv. Geophys.*, **21**, 87–230.

Smolarkiewicz, P. K., 1982: The multidimensional Crowley advection scheme. *Mon. Wea. Rev.*, **110**, 1968–1983.

Warming, R. F., P. Kutler and H. Lomax, 1973: Second- and third-order noncentered difference schemes for nonlinear hyperbolic equations. *AIAA J.*, **11**, 189–196.

——, and R. M. Beam, 1975: Upwind second-order difference schemes and applications in unsteady aerodynamic flows. *Proc. AIAA Second Computational Fluid Dynamics Conf.*, Hartford, CT, 17–28.

Zalesak, S. T., 1979: Fully multidimensional flux-corrected transport algorithms for fluids. *J. Comput. Phys.*, **31**, 335–362.